2007 IEEE International Conference on
Robotics and Automation
Roma, Italy, 10-14 April 2007

Vibration-Induced Frictional Force Fields on a Rigid Plate

Thomas H. Vose Paul Umbanhowar Kevin M. Lynch

Abstract— **By vibrating a rigid plate with up to six degrees of freedom, we can create a large family of programmable frictional force fields acting on parts resting on the plate. These fields can be used for sensorless part orientation, uncertainty-reducing transport, and simultaneous manipulation of multiple parts. The principle is demonstrated by a plate rotating about an axis below the plate. Simple oscillatory rotation produces a squeeze field that attracts and aligns parts along a center line. This behavior is confirmed in experiment. Motivated by this experimental confirmation, we use a simulation to find plate motions that yield a number of other useful primitive force fields. By sequencing these force fields, we can create any force field that is a convex combination of the primitives.**

I. Introduction

In pioneering work, Reznik and Canny [13], [14] demonstrated that vibration of a rigid plate in a horizontal plane can create frictional force fields acting on parts on the plate. These force fields arise because Coulomb friction forces between the plate and parts depend only on the direction of slip, the normal force, and the coefficient of friction, but not on the magnitude of the slip velocity. Based on this observation, asymmetric periodic plate motions can be designed that cause the plate to slip relative to a part for a longer time in one direction than another, producing a net force on the part in the first direction. By allowing the plate to rotate in the plane (not just translate), frictional force fields on the plate can be made position-dependent. Reznik and Canny exploited this property to build a three-degree-of-freedom vibratory plate that uses visual feedback to simultaneously drive multiple parts along independent trajectories.

We extend their work by considering a rigid vibratory plate that can move with six degrees of freedom. Out-of-plane motions allow us to change the effective gravitational force (and therefore friction force) experienced by a part during periodic motion of the plate. By using rotational motions to make this asymmetry position-dependent, we greatly increase the family of force fields that can be generated. In particular, Reznik and Canny's assumption that parts always slip relative to the plate, coupled with planar-only vibration, constrains the force field $\mathbf{f}$ to be *divergence free*, $\nabla \cdot \mathbf{f} = 0$. This means that the force field contains no sinks or sources, and that sensorless reduction in part uncertainty is not possible. In contrast, out-of-plane rotations allow the construction of programmable force fields that can position and orient parts without the use of sensors.

This work was supported by NSF grant IIS-0308224 and Thomas Vose's NSF fellowship.

Thomas Vose, Paul Umbanhowar, and Kevin Lynch are with the Department of Mechanical Engineering, Northwestern University, Evanston, IL 60208, USA {t-vose, umbanhowar, kmlynch}@northwestern.edu

For fixed automation, we can construct one- or two-degree-of-freedom versions that implement a subset of the full family of force fields that can be created by a six-degree-of-freedom plate. For example, the `LineSink` field (Section II), which squeezes parts to a center line, can be implemented using a single actuator. Using just two actuators, we can create a force field that pushes parts to a center line and translates them along that line. In both cases, parts with planar extent tend to be aligned with the center line. Two actuators also can be used to create shaped sink fields that approximate "universal" sensorless parts orienting fields, as demonstrated in theory [3], [7].

In [1], [4], parts are also oriented along a squeeze line on a vibrating plate. In that example, however, the plate is flexible, and the sink line is a node of the vibration. Parts interact with the plate by micro-impacts. In contrast, the part always remains in contact with the rigid plate in our system. We use a frictional sliding analysis and create force fields using the plate's rigid-body motion.

Programmable planar force fields have also been created using massively parallel arrays of actuators. These actuators include MEMS devices [2], air jets [6], rolling wheels [8], [10], [12], [11], and individual vibrating plates [5], [15]. In this last system, each individual plate translates in a circular motion in the horizontal plane and translates sinusoidally in the vertical direction. The phasing of these motions determines the force felt by parts on the plate—the net force is in the horizontal direction the plate is moving when the effective gravity is largest. These approaches to generating force fields differ from the work in this paper in that they require large numbers of individually-controlled actuators. In contrast, Luntz et al. [9], [16] use a small number of strategically-placed air sinks to position and orient laminar parts floating on an air bearing.

We begin in Section II by studying in detail how a squeeze field is generated by rotating a plate about an axis below the plate. The theoretical predictions are validated by experiment. Section III generalizes this behavior, describing how general plate and part motions give rise to steady-state velocity fields and zero-velocity force fields. In Section IV we examine primitive force fields created by simple plate motions. Sequencing primitives in time to produce a larger class of force fields is discussed in Section V. We conclude in Section VI by summarizing key points and discussing future directions.

1-4244-0602-1/07/$20.00 ©2007 IEEE.

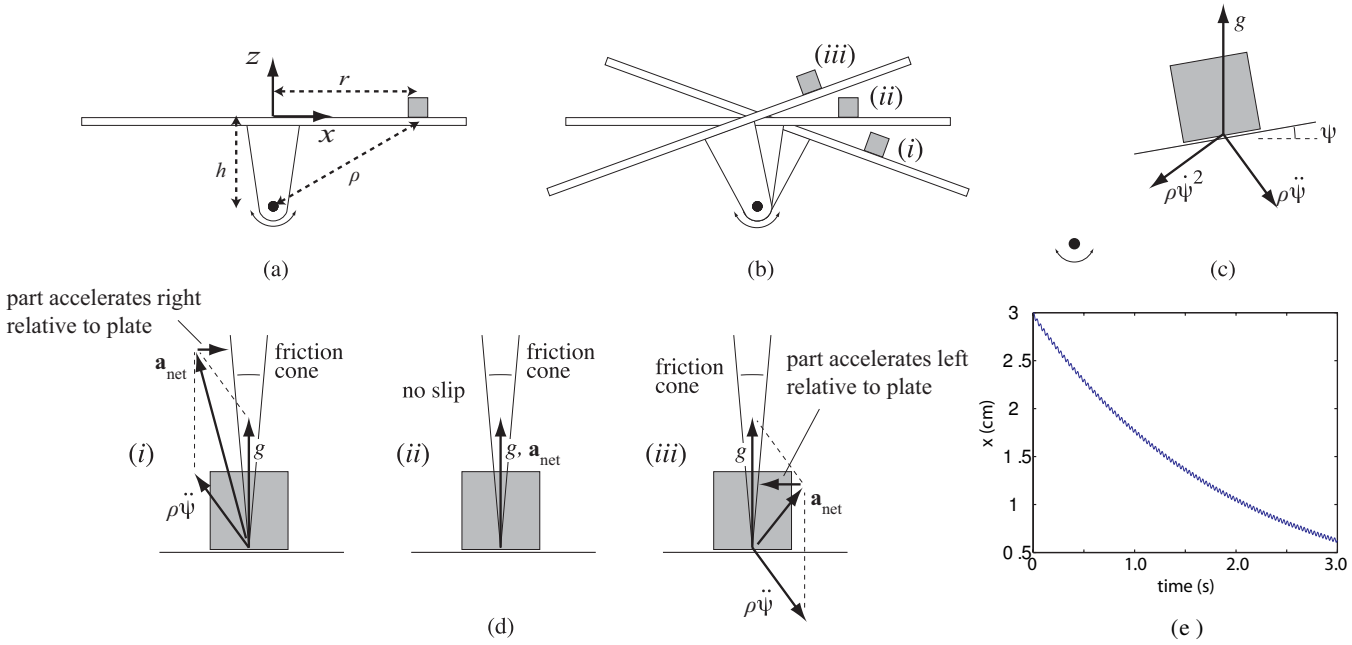

Fig. 1. (a) A part on a plate rotating about an axis below the plate in a gravitational field. A fixed inertial world frame with horizontal and vertical axes (x, z) is centered on the plate. (b) Three snapshots of the motion of the plate. The amount of rotation is exaggerated for clarity. (c) The acceleration of the contact point includes a centripetal component of magnitude $\rho\dot{\psi}^2$ and an angular component of magnitude $\rho\ddot{\psi}$. Considering only the part's motion relative to the plate, the gravitational field is equivalent to the plate accelerating upward with magnitude g. (d) Assuming $\psi = \dot{\psi} = 0$ (a good approximation for small amplitude, high frequency oscillation), the acceleration g is always normal to the plate and the only other acceleration component is $\rho\ddot{\psi}$. Let $\mathbf{a}_{\text{net}}$ be the total acceleration of the plate at the contact point with the part. At position (*i*) from (b), $\mathbf{a}_{\text{net}}$ lies to the left of the friction cone of possible accelerations of the point mass part. Therefore, a part initially stationary with respect to the plate begins to slip to the right relative to the plate with a small acceleration. At position (*iii*), a part initially at rest slips left relative to the plate with a larger acceleration. At position (*ii*), a part initially at rest does not slip. (e) The motion of a point part on the plate obtained from a simulation considering the full dynamics and stick-slip friction. Note the small-amplitude oscillatory motion as the part converges to the center of the plate. The plate is rotating sinusoidally with an amplitude of $0.3°$ at $f = 30$ Hz in full gravity, with an axis of rotation 5 cm below the plate.

II. The LineSink Primitive

We begin by analyzing a convergent squeeze field created by the one-degree-of-freedom rotational shaker device shown in Figure 1. The part rests on a horizontal plate that oscillates symmetrically (e.g., sinusoidally) about a perpendicular axis below the surface. At the contact point, the plate's acceleration has a centripetal component and a component due to the angular acceleration (see Figure 1(c)). The gravitational field is equivalent to a constant upward acceleration of the plate with magnitude g. Due to the high frequency, small amplitude nature of the plate's motion we are choosing to generate, we assume $\psi = \dot{\psi} = 0$. We also assume that the part is always slipping with respect to the plate.

The rotational motion of the plate causes the normal force on the part to vary in time throughout the cycle. For half of the cycle the right side of the plate is located below horizontal (represented by state (*i*) in Figure 1(b)). In this state, the effective gravity experienced by the part is greater than g, due to the plate's upward acceleration. During the other half of the cycle (state (*iii*)), the right side of the plate is above horizontal. In this state, the effective gravity experienced by the part is less than g due to the plate's downward acceleration.

In state (*i*), the net acceleration of the plate lies just to the left of the part's friction cone due to the increased normal force (Figure 1(d)); from the part's perspective, the plate has a small acceleration to the left. Therefore, a part initially at rest will begin to slip slightly to the right relative to the plate. In state (*iii*), the net acceleration of the plate lies to the right and farther from the edge of the friction cone due to the decreased normal force. A part at rest will slip to the left relative to the plate with a larger acceleration than in state (*i*). The net effect is that the part slides towards the axis of rotation over the course of one cycle. We call this behavior a `LineSink`. Results from a numerical simulation are shown in Figure 1(e).

If the axis of rotation is placed *above* the plate surface, the situation is reversed; the part will slide *away* from the axis of rotation over the course of a cycle. We call this behavior a `LineSource`.

A. Steady-State Velocity

The notion of a steady-state velocity is useful for characterizing the behavior of point parts on the plate. When the part's velocity at the end of the cycle matches its velocity at the beginning of the cycle, we say it is in steady-state. We define the steady-state velocity as the average velocity of the part over a steady-state cycle. This notion is an approximate one, as we assume the part's motion during the cycle is negligible. However, simulations indicate that point parts rapidly approach steady state behavior regardless of their

initial velocity and position.

For certain plate motions it is possible to find a closed-form solution of the steady-state velocity; one such case is for the device shown in Figure 1. In particular, let the angular acceleration of the plate, $\ddot{\psi}(t)$, be a square wave of period T defined by

$$\ddot{\psi}(t) = \begin{cases} \alpha & 0 \le t < T/2 \\ -\alpha & T/2 \le t < T. \end{cases} \quad (1)$$

Call the vertical distance from the axis to the plate h and the horizontal distance from the axis to the part r. With the approximation $\psi = \dot{\psi} = 0$, the acceleration of the plate at the contact point with the part has horizontal and vertical components

$$a_{s_x}(t) = -h\alpha,\ a_{s_z}(t) = r\alpha \quad 0 \le t < T/2 \quad (2)$$
$$a_{s_x}(t) = h\alpha,\ a_{s_z}(t) = -r\alpha \quad T/2 \le t < T \quad (3)$$

in the fixed world frame defined by (x, z).

The effective gravity experienced by the part is defined as

$$g_{\text{eff}}(t) = g + a_{s_z}(t). \quad (4)$$

We assume that the displacement of the part is negligible over a single cycle so that the effective gravity is a piecewise constant function in time.

We impose two restrictions to obtain an analytical solution for the steady-state velocity. First, we require that $g_{\text{eff}} \ge 0$ for all time so that the part never loses contact with the plate. This condition bounds the distance $r_{\max}$ for which the steady-state analysis is defined:

$$r \le r_{\max} = \frac{g}{\alpha}.$$

The second restriction is that the part never sticks to the plate. This condition is satisfied if at all times

$$|a_{s_x}| > \mu g_{\text{eff}},$$

where μ is the friction coefficient. As the maximum value of g_{eff} is $g + r\alpha$, this condition is satisfied if

$$h\alpha > \mu(g + r\alpha).$$

Figure 2 shows steady-state velocity profiles, $v_{p_x}(t)$ and $v_{s_x}(t)$, for the part and the plate over one cycle. Without loss of generality, we start the plate at rest in state (*iii*) from Figure 1(b). During the first quarter of the cycle (state (*iii*)), the plate accelerates away from the part, resulting in a small value of g_{eff}; the acceleration of the part is $\mu(g - r\alpha)$. During the middle half of the cycle (state (*i*)), the plate is accelerating upward, which leads to a higher value of g_{eff}; the magnitude of the acceleration of the part is $\mu(g + r\alpha)$. Once the part's velocity matches the plate's (at C), its acceleration changes from positive to negative. For the last quarter of the cycle (state (*iii*)), g_{eff} is once again low; the magnitude of the acceleration of the part reverts back to $\mu(g - r\alpha)$. At E the part's velocity instantaneously matches the plate's for the second time, forcing the acceleration to change from negative back to positive.

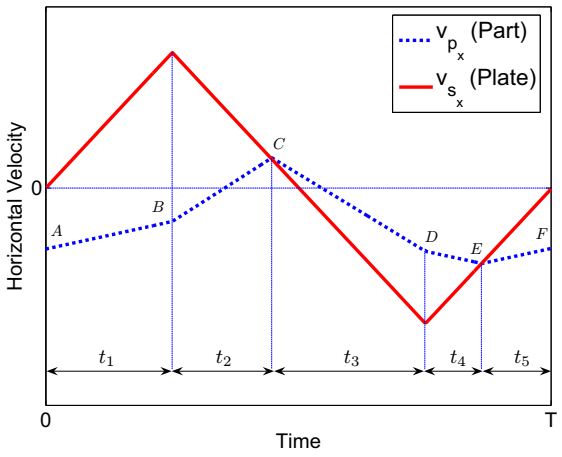

Fig. 2. Steady-state velocity profiles for the plate and the part in the horizontal direction.

Using the notation of Figure 2 we can write expressions for the velocity of the part at points A–F,

$$v_B = v_A + \mu(g - r\alpha)t_1 \quad (5)$$
$$v_C = v_B + \mu(g + r\alpha)t_2 \quad (6)$$
$$v_D = v_C - \mu(g + r\alpha)t_3 \quad (7)$$
$$v_E = v_D - \mu(g - r\alpha)t_4 \quad (8)$$
$$v_F = v_E + \mu(g - r\alpha)t_5 \quad (9)$$
$$v_A = v_F. \quad (10)$$

Equating the final and initial velocities in (10) ensures that the part is in steady state.

The three equations that relate the times are:

$$t_1 = \frac{1}{4}T \quad (11)$$
$$t_2 + t_3 = \frac{1}{2}T \quad (12)$$
$$t_4 + t_5 = \frac{1}{4}T. \quad (13)$$

Since the maximum plate speed is $\frac{1}{4}h\alpha T$ and the velocities of the part and plate are equal at points C and E, we obtain two more equations:

$$v_C = \frac{1}{4}h\alpha T - h\alpha t_2 \quad (14)$$
$$v_E = -\frac{1}{4}h\alpha T + h\alpha t_4. \quad (15)$$

The average steady-state velocity of the part over the cycle is

$$v_{\text{ss}} = \frac{1}{T}\left(\frac{v_A + v_B}{2}t_1 + \frac{v_B + v_C}{2}t_2 + \frac{v_C + v_D}{2}t_3 + \frac{v_D + v_E}{2}t_4 + \frac{v_E + v_A}{2}t_5\right) \quad (16)$$

which reduces to

$$v_{\text{ss}} = \frac{\mu^2[g^2 - (r\alpha)^2] - 3(h\alpha)^2}{8(h\alpha)^2}\alpha\mu r T \quad (17)$$

when substituting (5) through (15).

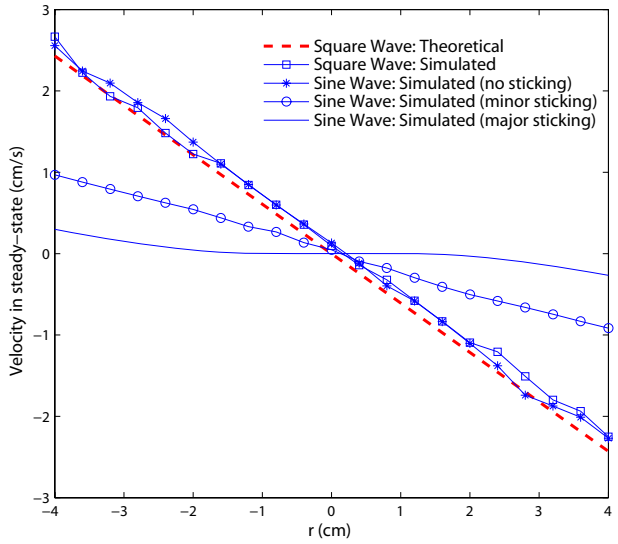

Fig. 3. When the plate is oscillated about an axis below the surface with either a square or sine wave angular acceleration profile, the relationship between the part's steady-state velocity and its distance from the axis is nearly linear. In all five cases shown, $T = 0.03$ s and $\mu = 0.3$. The theoretical square wave plot is based on equation (21) with $\alpha = 180$ rad/s^2. The four simulated plots incorporate the full dynamics, allowing part position and effective gravity to change during the cycle. The simulated square wave has $\alpha = 180$ rad/s^2 with $h = 5$ cm. The three sine waves all have angular accelerations with amplitude 220 rad/s^2. The simulated sine wave (no sticking) has $h = 5$ cm. The simulated sine wave (minor sticking) has $h = 2$ cm. The simulated sine wave (major sticking) has $h = 1$ cm.

The r terms can be factored out to yield

$$v_{ss} = br + cr^3 \tag{18}$$

where b and c are constants:

$$b = \frac{\mu T}{8h^2\alpha}(\mu^2 g^2 - 3h^2\alpha^2) \tag{19}$$

$$c = \frac{\mu^3 \alpha T}{8h^2}. \tag{20}$$

Under typical operating conditions ($\alpha \sim 10^2$ rad/s^2), the linear term in (18) dominates because the part must be close to the axis of rotation to avoid losing contact with the plate ($r \ll 1$ m). Additionally, if the vertical distance from the axis to the plate (h) is too small, the part will stick to the plate. Thus, it is reasonable to assume that $\mu^2 g^2 \ll 3h^2\alpha^2$. With these simplifications, (18) reduces to

$$v_{ss} \approx -\frac{3\mu T \alpha}{8} r. \tag{21}$$

The steady-state velocity of the part is always directed towards the axis of rotation and increases linearly with distance. The rate of convergence to the axis can be controlled by adjusting T or α.

Numerical simulations indicate that nearly linear behavior also occurs when the vibration is sinusoidal (Figure 3). In fact, if the axis of rotation is far enough below the plate surface to ensure that the part never sticks, the steady-state velocities for square and sine wave angular accelerations are almost indistinguishable, and closely follow the theoretical curve of (21). Even if the axis of rotation is moved closer to the plate and causes the part to stick for a small portion of the cycle, a sinusoidal angular acceleration still results in linear behavior. However, when the axis is moved too close to the plate (h is small), the part may come to rest before $r = 0$. In this deadband region, the effective gravity never becomes small enough to allow the part to slip, given the decreased side-to-side acceleration due to small h.

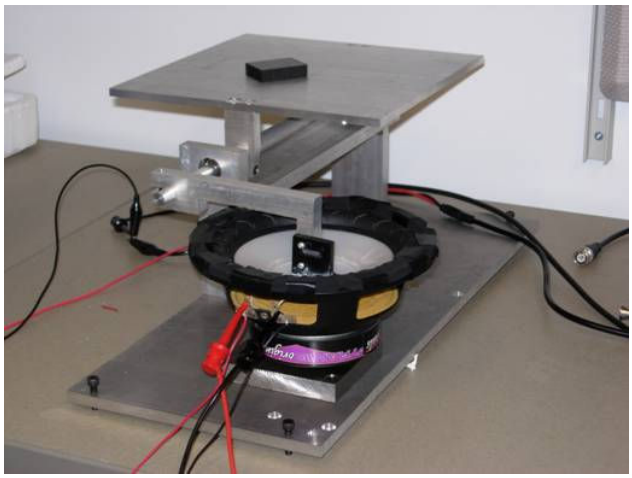

Fig. 4. One-degree-of-freedom shaker device with rotation axis below the plate surface. Linear motion of a speaker is converted into rotational motion of the plate.

B. Experimental Results

We used the one-degree-of-freedom rotational shaker device shown in Figure 4 to experimentally study the relationship between the part's velocity and its distance r from the axis of rotation. The shaker plate is made of aluminum. The axis of the rotation is located 4 cm below the plate surface. It is driven by a speaker whose linear motion is converted into rotational motion through a lever arm. A function generator provides a sinusoidal input signal to a stereo amplifier which powers the speaker. An accelerometer mounted on the plate verifies nearly sinusoidal acceleration of the plate surface.

The part was an aluminum disk with a diameter of 0.5 cm. It was initially placed at rest 9 cm from the axis of rotation and allowed to move inwards. Timing began when the center of the part was 6.5 cm from the axis. The time was recorded after every 0.5 cm of travel between 6.5 cm and 1 cm. Recordings were not taken until the part reached the 6.5 cm mark because it audibly rattled when located between 7.5 and 9 cm, indicating loss of contact with the plate. Once inside 7.5 cm, the part appeared to travel very smoothly, with virtually no rotational motion.

For `LineSink`-type behaviors that have the form

$$v(r) = -kr$$

such as (21), the time it takes for a part to move from an initial position, r_0, to a final position, r, is given by

$$t = \frac{1}{k} \ln \frac{r_0}{r}. \tag{22}$$

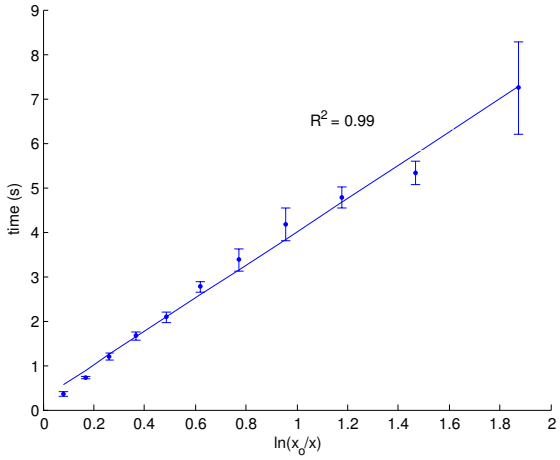

Fig. 5. Data taken with the shaker shown in Figure 4. The shaker was driven with a roughly sinusoidal angular acceleration. A small part traveled to the center of the plate and was timed every 0.5 cm. Error bars indicate the spread of ten trials.

Therefore, a plot of t vs. $\ln \frac{r_0}{r}$ should produce a line. The experimental data is plotted in Figure 5. Ten trials were performed and the plotted points represent average times. A line was fitted to the data with $R^2 = 0.99$, confirming a strong linear relationship between the part location and the part velocity.

Video of rectangular parts in a `LineSink` field can be viewed at http://lims.mech.northwestern.edu/∼lynch/research/videos/feeding.html. These parts, which have significant planar extent, tend to orient themselves along the sink line as they move towards the center of the plate.

III. Turning Plate Motion into Fields

One goal of our work is to be able to design a plate vibration that produces a desired field. The analysis of Section II yielded a steady-state velocity field for `LineSink`. A point part on the plate tends to follow the integral curves of this velocity field, in this case moving directly toward a center line with decreasing velocity. Another type of field is a zero-velocity force field. This field represents the net force experienced by a point part of unit mass at rest. While the interpretations of the steady-state velocity field and the zero-velocity force field are different, they often look nearly identical.

One way to approximate the zero-velocity force field at a point is to measure the acceleration of a part starting from rest, averaged over a small number of cycles. We envision this field being particularly useful for determining equilibrium part orientations.

It is worth noting that, for some fields, the part must be allowed to move during the cycle in order for it to feel a net force. For example, in the `LineSink` example of the previous section, if the part were held stationary at $r \neq 0$, the net force on the part over the cycle would be zero, whereas it would be nonzero if the part began at rest but were free to move during the cycle.

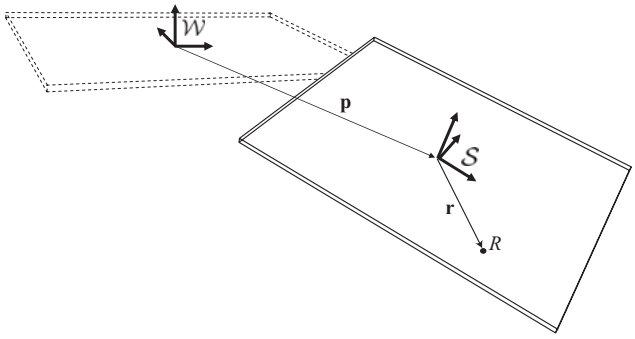

Fig. 6. The dashed plate on the left is in the horizontal home position; its center is aligned with the origin of the fixed inertial frame $\mathcal{W}$. The solid plate is in an arbitrary position.

A. Plate Motion

We define a fixed inertial frame $\mathcal{W}$ and a frame $\mathcal{S}$ attached to the origin of the plate (Figure 6). The two frames coincide when the plate is in the horizontal home position. The configuration of the plate in $\mathcal{W}$ is given by

$$\begin{bmatrix} \mathbf{R}(t) & \mathbf{p}(t) \\ 0 & 1 \end{bmatrix} \in SE(3),$$

where $\mathbf{p} : \mathbb{R} \to \mathbb{R}^3$ and $\mathbf{R} : \mathbb{R} \to SO(3)$ are both C^1 functions of time. The motion of the plate is periodic with period T, so that $(\mathbf{p}(t), \mathbf{R}(t)) = (\mathbf{p}(t+T), \mathbf{R}(t+T))$.

Let $\mathbf{r} = [r_x, r_y, 0]^T$ be a vector in the plate frame $\mathcal{S}$ to the point R on the plate. The location of R in $\mathcal{W}$ is written $\mathbf{r}_\mathcal{W}$, with

$$\begin{aligned} \mathbf{r}_\mathcal{W} &= \mathbf{R}\mathbf{r} + \mathbf{p} \\ \dot{\mathbf{r}}_\mathcal{W} &= \omega \times \mathbf{R}\mathbf{r} + \dot{\mathbf{p}} \\ \ddot{\mathbf{r}}_\mathcal{W} &= \omega \times \omega \times \mathbf{R}\mathbf{r} + \alpha \times \mathbf{R}\mathbf{r} + \ddot{\mathbf{p}}, \end{aligned}$$

where ω and α are, respectively, the angular velocity and acceleration of the plate. The plate's velocity and acceleration at R can then be expressed in an inertial frame $\mathcal{S}'$, instantaneously aligned with $\mathcal{S}$, as

$$\mathbf{v}_s = \mathbf{R}^T \dot{\mathbf{r}}_\mathcal{W} \quad (23)$$

$$\mathbf{a}_s = \mathbf{R}^T \ddot{\mathbf{r}}_\mathcal{W}. \quad (24)$$

B. Friction Forces

Let $\mathbf{v}_s(\mathbf{r}, t)$ be the velocity of the plate surface at a point R in an inertial frame $\mathcal{S}'$ instantaneously aligned with the plate frame. Let a point mass part located at R have velocity $\mathbf{v}_p$ in $\mathcal{S}'$ and be in contact with the plate. The force exerted on the part depends upon the relative velocity between the part and the plate, $\mathbf{v}_{\text{rel}} = \mathbf{v}_p - \mathbf{v}_s$.

If we assume the part is slipping with respect to the plate ($\mathbf{v}_{\text{rel}} \neq 0$), the part will experience a force $\mathbf{f}$ due

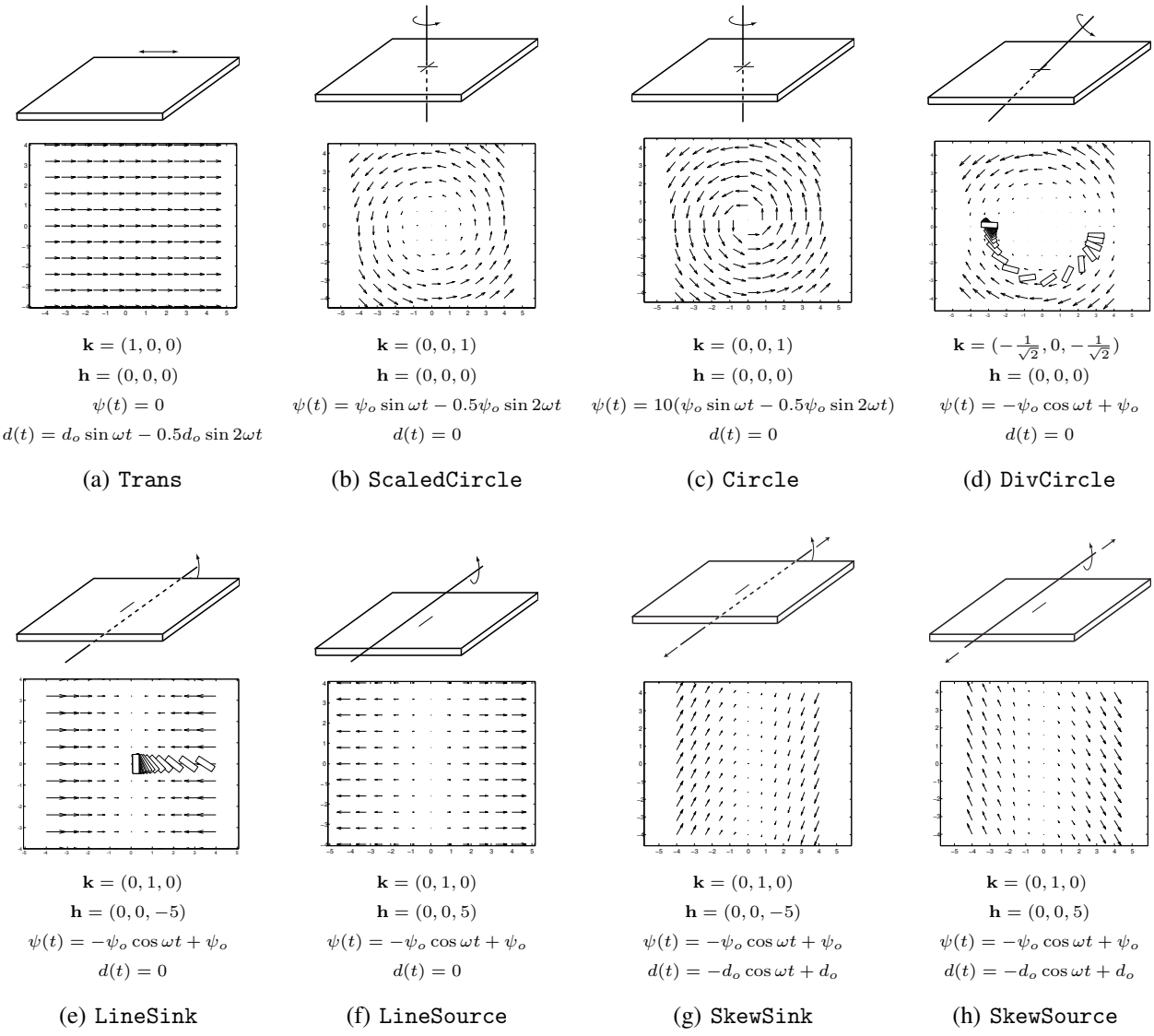

Fig. 7. Each of (a)-(e) shows a perspective view of a horizontal plate and its motion generating a primitive force field. The elements of $\mathbf{h}$ are given in centimeters. The other parameters are: $\omega = 209$ rad/s ($T = 0.03$ s), $\psi_o = 0.005$ radians, and $d_o = 0.05$ cm. The simulated motions of a uniform mass rectangle overlaid on top of the force fields are shown in (d) and (e).

to kinetic friction in the direction opposite to the relative velocity vector,

$$\mathbf{f} = -\mu_k m g_{\text{eff}} \frac{\mathbf{v}_{\text{rel}}}{\|\mathbf{v}_{\text{rel}}\|}, \tag{25}$$

where μ_k is the coefficient of kinetic friction, m is the mass of the part, and g_{eff} is the sum of the z-component of the plate's acceleration and the negative of the gravitational acceleration projected to the z-axis.

If the relative velocity between the part and the plate is zero, the part is stuck to the plate and experiences a force due to static friction. If the tangential acceleration of the plate is less than $\mu_s g_{\text{eff}}$, where μ_s is the static friction coefficient, the part remains fixed to the plate. Otherwise, the part begins to slip. In this case, the friction force has a magnitude of $\mu_s m g_{\text{eff}}$ in the direction of the plate's tangential acceleration.

C. Simulator

We have created a program in Matlab to approximate steady-state velocity and zero-velocity force fields for a given plate motion, as well as to simulate the motion of a part with planar extent. The simulation takes into account the full part dynamics as long as contact with the plate is maintained.

Calculating zero-velocity force (acceleration) fields can be problematic because the part's behavior over a small number of cycles is sensitive to the initial velocity of the plate. To mitigate this effect, we initialize the simulation with the part at rest at 30 different points within the plate's motion cycle. For each of these 30 initial conditions, we average the acceleration over one cycle. The 30 average accelerations are then averaged to give the approximate acceleration of the part. Repeating this procedure over a discrete set of points

TABLE I
APPROXIMATE FORCE FIELD REPRESENTATIONS OF THE MOTION PRIMITIVES

Primitive	Force Field
`Trans`	$\mathbf{f}(x,y) \approx a(1,0)$
`ScaledCircle`	$\mathbf{f}(x,y) \approx a(-y,x)$
`Circle`	$\mathbf{f}(x,y) \approx a\left(\frac{-y}{\sqrt{x^2+y^2}}, \frac{x}{\sqrt{x^2+y^2}}\right)$
`DivCircle`	$\mathbf{f}(x,y) \approx (axy, bx^2)$
`LineSink`	$\mathbf{f}(x,y) \approx a(-x,0)$
`LineSource`	$\mathbf{f}(x,y) \approx a(x,0)$
`SkewSink`	$\mathbf{f}(x,y) \approx a(-x,x)$
`SkewSource`	$\mathbf{f}(x,y) \approx a(x,-x)$

gives a sense of the force field.

IV. MOTION PRIMITIVES

To find a set of primitive force fields, we have investigated a set of motion primitives consisting of periodic screw motions. Each primitive is defined by a rotation axis $\mathbf{k}$ in $\mathcal{W}$, a point $\mathbf{h}$ through which $\mathbf{k}$ passes, a periodic translation $d(t)$ along $\mathbf{k}$, and a periodic rotation $\psi(t)$ about $\mathbf{k}$. Eight primitive fields are shown in Figure 7 along with their $\{\mathbf{k}, \mathbf{h}, \psi(t), d(t)\}$ representations.

The first three primitives are generated from purely in-plane plate motion, as in [13], [14]. Asymmetrical longitudinal motion produces `Trans`; the magnitude of the force is constant everywhere on the plate. Asymmetrical rotational motion produces `ScaledCircle` and `Circle`. In the `Circle` field, the magnitude of the force is nearly independent of plate location due to very large plate velocities [13]. In the `ScaledCircle` field, the magnitude of the force is roughly proportional to the distance from the rotation axis. This behavior occurs when the plate's velocity is of the same order of magnitude as the part's.

The fourth primitive, `DivCircle`, results from symmetric rotation about an axis that pierces the plate at a $45°$ angle. Where the axis is above the plate, the field is divergent like `LineSource`; where the axis is below the plate it is convergent like `LineSink`.

The next two primitives, `LineSink` and `LineSource`, discussed in section II, are created by symmetric rotation about an axis below and above the plate, respectively.

Full screw motions about an axis (simultaneous rotation and translation with the same phase and frequency) above and below the plate surface produce the final two primitives, `SkewSink` and `SkewSource`.

Approximate closed-form representations for the force fields based on simulation data are given in Table I. The positions and orientations of these fields can be modified by changing the positions and orientations of the motion axes.

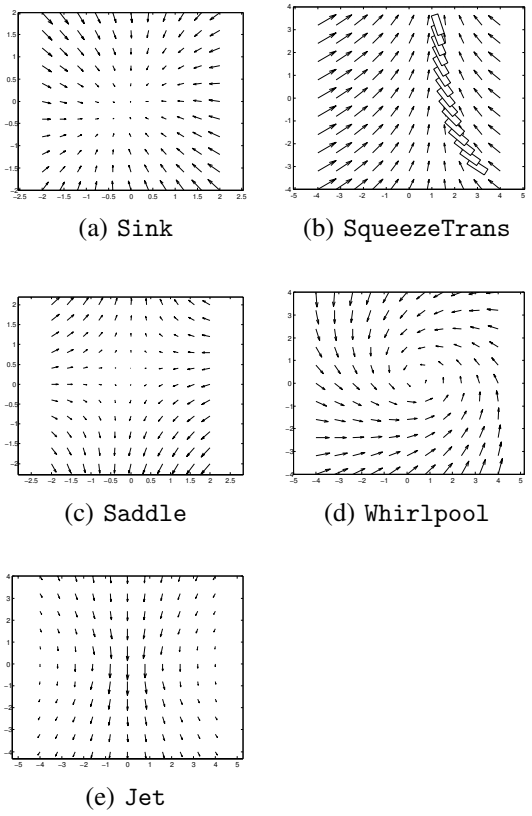

Fig. 8. Results of sequencing the motion primitives from Figure 7 are shown in (a)-(e). In each case, the next motion primitive begins the instant the previous one ends. The simulated motion of a uniform mass rectangle is shown overlaid on top of the force field in (b).

V. COMBINING MOTION PRIMITIVES

We can concatenate the primitives in time, provided the trajectories at the points of "gluing" have continuous velocities and positions. By concatenating primitive force fields, we can achieve time-averaged force fields, vastly expanding the class of obtainable fields. The simulated fields in Figure 8 are representative. All of them were created by combining primitive motions from Figure 7. Since all the primitive motions are defined such that the plate begins and ends at rest in the horizontal home position, smooth sequencing is ensured.

Two orthogonal `LineSinks` sequenced one after the other produce a `Sink`. This is a close approximation to the elliptic field for parts orienting in [4]. Sequencing a `LineSink` and a linear transport `Trans` produces a `SqueezeTrans`, which may be useful for simultaneous orientation and transport. A `LineSink` and a `LineSource` create a `Saddle`. Other fields include a `Whirlpool` (two orthogonal `LineSinks` and a `Circle`), and a `Jet` for localized transport (two `Circles`) [14]. Once a sufficiently rich set of primitive fields has been developed, generating a desired field amounts to finding an appropriate sequence of scaled primitives.

In theory, the set of all convex combinations of primitive

force fields in Table I are obtainable by sequencing primitives in time. In practice, however, each primitive has a basic "quantum" unit consisting of a full cycle. Therefore, time-averaging of the fields is only approximate; the part may move significantly before the next primitive is applied, so that the net result is only approximately modeled by a time-averaged field. In addition, there is an interaction between the motion primitives depending on the order in which they are executed; the sliding motion at the end of one motion primitive will influence the effect of the next motion primitive. To lessen this effect, the motion primitives may be joined by a period during which the plate is at rest. This reduces the strength of the combined force field, however. When a rest period is not included, we see slight asymmetries in the simulated time-averaged force field relative to our prediction. For example, we would predict that the squeeze line of the `SqueezeTrans` field of Figure 8 would be centered on the plate based on the two individual primitives. The fact that it is not illustrates an offset that depends on the phasing of the two primitives.

VI. Conclusions and Future Work

We have shown how to create force and velocity fields with nonzero divergence by vibration of a rigid plate. In particular, a squeeze field can be created by symmetric oscillation about an axis below the plate (`LineSink`). In both simulation and experiment, this field was shown to obey an approximately linear relationship between part velocity and distance from the axis of rotation. Further, the strength of the field and the location of the squeeze line are easily controllable in a six-degree-of-freedom implementation. By sequencing two orthogonal squeeze fields to make a `Sink` field, it is possible to sensorlessly orient parts on a vibrating plate. We are currently in the process of building a six-degree-of-freedom shaker to test this and our other simulation results. We also plan to continue to build a library of force field primitives by investigating new types of plate motion. The convex combination of primitive force fields describes a large family of time-averaged force fields that we plan to characterize in more detail.

The zero-velocity force (or acceleration) fields described in this paper can be used to determine equilibrium configurations of parts with planar extent. To do this, we can "lift" the pointwise force field to a force field in the three-dimensional configuration space describing the part's position and orientation on the plate. This requires integrating over the part the product of the acceleration field and the part's support pressure distribution. In most past work, the part's support distribution is assumed uniform, allowing precise calculation of equilibria. As the support distribution is usually underdetermined, however, the best we can hope for is to calculate tight bounds on the possible equilibrium set. This is an area for future work.

Acknowledgment

We would like to thank Dan Sheehan for constructing the device used for the experiments.

References

[1] K. F. Böhringer, V. Bhatt, and K. Y. Goldberg. Sensorless manipulation using transverse vibrations of a plate. In *IEEE International Conference on Robotics and Automation*, pages 1989–1996, 1995.

[2] K.-F. Böhringer, B. Donald, and N. MacDonald. Sensorless manipulation using massively parallel microfabricated actuator arrays. In *IEEE International Conference on Robotics and Automation*, 1994.

[3] K.-F. Böhringer, B. R. Donald, L. E. Kavraki, and F. Lamiraux. A single universal force field can uniquely orient non-symmetric parts. In *International Symposium on Robotics Research*, pages 395–402. Springer, 1999.

[4] K.-F. Böhringer, L. Kavraki, and F. Lamiraux. Part orientation with one or two stable equilibria using programmable force fields. *IEEE Trans. Robot. Autom.*, 16:157–170, Apr 2000.

[5] P. U. Frei, M. Wiesendanger, R. Büchi, and L. Ruf. Simultaneous planar transport of multiple objects on individual trajectories using friction forces. In K. F. Böhringer and H. Choset, editors, *Distributed Manipulation*, pages 49–64. Kluwer Academic Publishers, 2000.

[6] S. Konoshi and H. Fujita. A conveyance system using air flow based on the concept of distributed micro motion systems. *Journal of Microelectromechanical Systems*, 3(2):54–58, 1994.

[7] F. Lamiraux and L. Kavraki. Positioning symmetric and non-symmetric parts using radial and constant force fields. In *Workshop on the Algorithmic Foundations of Robotics*, 2000.

[8] J. Luntz, W. Messner, and H. Choset. Velocity field design for parcel manipulation on the modular distributed manipulator system. In *IEEE International Conference on Robotics and Automation*, 1999.

[9] J. Luntz and H. Moon. Distributed manipulation with passive air flow. In *IEEE/RSJ International Conference on Intelligent Robots and Systems*, 2001.

[10] J. E. Luntz, W. Messner, and H. Choset. Distributed manipulation using discrete actuator arrays. *International Journal of Robotics Research*, 20(7), July 2001.

[11] T. Murphey and J. Burdick. Feedback control for distributed manipulation systems that involve mechanical contacts. *International Journal of Robotics Research*, 23(7):763–781, July 2004.

[12] T. D. Murphey and J. W. Burdick. Global exponential stabilizability for distributed manipulation. In *IEEE International Conference on Robotics and Automation*, Washington D.C., 2002.

[13] D. Reznik and J. Canny. A flat rigid plate is a universal planar manipulator. In *IEEE International Conference on Robotics and Automation*, pages 1471–1477, 1998.

[14] D. Reznik and J. Canny. C'mon part, do the local motion! In *IEEE International Conference on Robotics and Automation*, pages 2235–2242, 2001.

[15] L. S. Ruf, P. Frei, and M. Wiesendanger. US Patent #6,189,677, SIG Pack Systems AG, Feb 2001.

[16] K. Varsos, H. Moon, and J. Luntz. Generation of quadratic potential force fields from flow fields for distributed manipulation. *IEEE Transactions on Robotics*, 22(1):108–118, Feb. 2006.